# Engineering of a membrane-triggered activity switch in coagulation factor VIIa

Anders L. Nielsen[a], Anders B. Sorensen[a], Heidi L. Holmberg[a], Prafull S. Gandhi[a], Johan Karlsson[a], Jens Buchardt[a], Kasper Lamberth[a], Mads Kjelgaard-Hansen[a], Carsten Dan Ley[a], Brit B. Sørensen[a], Wolfram Ruf[b,c], Ole H. Olsen[a], and Henrik Østergaard[a,1]

[a]Global Research, Novo Nordisk A/S, DK-2760 Maaloev, Denmark; [b]Department of Immunology and Microbial Science, The Scripps Research Institute, La Jolla, CA 92037; and [c]Center For Thrombosis and Hemostasis, University Medical Center, 55131 Mainz, Germany

Edited by Robert J. Fletterick, University of California, San Francisco School of Medicine, San Francisco, CA, and approved October 6, 2017 (received for review November 11, 2016)

**Recombinant factor VIIa (FVIIa) variants with increased activity offer the promise to improve the treatment of bleeding episodes in patients with inhibitor-complicated hemophilia. Here, an approach was adopted to enhance the activity of FVIIa by selectively optimizing substrate turnover at the membrane surface. Under physiological conditions, endogenous FVIIa engages its cell-localized cofactor tissue factor (TF), which stimulates activity through membrane-dependent substrate recognition and allosteric effects. To exploit these properties of TF, a covalent complex between FVIIa and the soluble ectodomain of TF (sTF) was engineered by introduction of a nonperturbing cystine bridge (FVIIa Q64C-sTF G109C) in the interface. Upon coexpression, FVIIa Q64C and sTF G109C spontaneously assembled into a covalent complex with functional properties similar to the noncovalent wild-type complex. Additional introduction of a FVIIa-M306D mutation to uncouple the sTF-mediated allosteric stimulation of FVIIa provided a final complex with FVIIa-like activity in solution, while exhibiting a two to three orders-of-magnitude increase in activity relative to FVIIa upon exposure to a procoagulant membrane. In a mouse model of hemophilia A, the complex normalized hemostasis upon vascular injury at a dose of 0.3 nmol/kg compared with 300 nmol/kg for FVIIa.**

coagulation | factor VIIa | tissue factor | serine proteases | disulfide engineering

The cascade of proteolytic events serving to restore hemostasis upon vascular injury is initiated by assembly of the complex between coagulation factor VIIa (FVIIa) and its cell-surface receptor tissue factor (TF) (reviewed in refs. 1 and 2). Cofactor binding is facilitated by extended surface interactions with FVIIa, in which the N-terminal γ-carboxy glutamic acid (Gla) -rich domain, the two epidermal growth factor like domains (EGF1 and -2), and the protease domain all participate (2, 3). In addition to providing membrane anchoring, TF binding serves to optimally orient and present FVIIa for efficient proteolytic processing of its two physiological substrates, factor IX and X (FIX and FX) (4, 5). These initial proteolytic events trigger the downstream coagulation response, which ultimately leads to thrombin generation and the formation of a fibrin plug.

The mechanistic basis for the cofactor function of TF has been delineated by structural, mutational, and kinetic studies and can be divided into contributions originating from allosteric effects on FVIIa and direct interactions with the substrates. Both features are recapitulated by the soluble ectodomain of TF (sTF) (6, 7) and is evident as a four to five orders-of-magnitude enhancement of FX turnover in the presence of sTF and a procoagulant membrane surface (8).

TF binding stimulates the intrinsic catalytic activity of FVIIa by facilitating a conformational transition of the protease domain from a state with predominantly zymogen-like features into a catalytically competent form (9, 10). The conformational activation follows the typical paradigm of trypsin-like serine protease activation and involves formation of the N-terminal I153-D343 (FVII numbering) salt bridge and reorientation of loops to mature the active site (11). The transition can be monitored by conformation-specific antibodies and protection of I153 from chemical modification and results in a 30- to 50-fold increased amidolytic activity and reactivity with the plasma inhibitor antithrombin (AT) (6, 10, 12–14). Transmission of the allosteric signal across the FVIIa–TF interface is critically dependent on residue M306 in the protease domain of FVIIa (corresponding to position 164 in chymotrypsin), which upon substitution abrogates allosteric activation while maintaining cofactor affinity (15, 16).

Engagement of macromolecular substrates by the FVIIa–TF complex is driven by interactions involving exosites remote from the active site (5). On TF, a membrane proximal patch has been defined and distinct recognition sites have been localized on FVIIa (17–19). Since the enhancement of proteolytic activity by sTF in solution is only a few hundred-fold, of which allosteric activation accounts for the major part (15, 20), exosite-mediated FX recognition appears to be realized primarily on the membrane surface.

With ∼400,000 people affected worldwide, hemophilia is one of the most frequent hemostatic disorders. Standard therapy entails replenishment of the deficient factor VIII (FVIII) or IX; however, in about 30% of the cases, substitution therapy is rendered ineffective due to the development of neutralizing alloantibodies (inhibitors) (21). Recombinant FVIIa is an approved treatment option under these circumstances. Several lines of evidence

## Significance

**Coagulation factor VIIa (FVIIa) is an intrinsically poor serine protease that requires assistance from its cofactor tissue factor (TF) to trigger the extrinsic pathway of blood coagulation. TF stimulates FVIIa through allosteric maturation of its active site and by facilitating substrate recognition. The surface dependence of the latter property allowed us to design a potent membrane-triggered activity switch in FVIIa by engineering a disulfide cross-link between an allosterically silent FVIIa variant and soluble TF. These results show that optimization of substrate recognition remote from the active site represents a promising new route to simultaneously enhance and localize the procoagulant activity of FVIIa for therapeutic purposes.**

Author contributions: A.L.N., A.B.S., H.L.H., P.S.G., J.B., K.L., M.K.-H., C.D.L., B.B.S., W.R., O.H.O., and H.Ø. designed research; A.L.N., A.B.S., H.L.H., K.L., M.K.-H., C.D.L., B.B.S., W.R., O.H.O., and H.Ø. performed research; J.K. contributed new reagents/analytic tools; A.L.N., A.B.S., H.L.H., P.S.G., J.B., K.L., M.K.-H., C.D.L., B.B.S., W.R., O.H.O., and H.Ø. analyzed data; and A.L.N., A.B.S., and H.Ø. wrote the paper.

Conflict of interest statement: A.L.N., A.B.S., H.L.H., P.S.G., J.B., K.L., M.K.-H., C.D.L., B.B.S., O.H.O., and H.Ø. are employed by Novo Nordisk A/S.

This article is a PNAS Direct Submission.

This open access article is distributed under Creative Commons Attribution-NonCommercial-NoDerivatives License 4.0 (CC BY-NC-ND).

[1]To whom correspondence should be addressed. Email: hqsg@novonordisk.com.

This article contains supporting information online at www.pnas.org/lookup/suppl/doi:10.1073/pnas.1618713114/-/DCSupplemental.

support a mechanism by which the pharmacological effect of FVIIa is exerted primarily through direct activation of FX on the activated platelet surface independent of TF (22–24). Because of the poor activity of free FVIIa, various approaches for optimizing its hemostatic potential have been pursued and shown promise in terms of improved treatment efficacy of bleeding episodes in animal models and recently in patients (25–28).

Here, we have explored an approach to increase the procoagulant activity of FVIIa in a localized manner, by utilizing the ability of sTF to preferentially facilitate macromolecular substrate recognition on the membrane surface.

## Results

**Design of Disulfide-Linked FVIIa–sTF Complexes.** Based on a geometric analysis (29) of the energy minimized crystal structure of the FVIIa–sTF complex (3), two residue pairs across the interface were predicted to be suitable for disulfide engineering (the noncovalent complex is denoted FVIIa+sTF in the following). Further analysis of a 20-ns molecular dynamics (MD) simulation of the complex identified seven additional residue pairs obeying the geometric requirements for disulfide bond formation (Fig. 1*A* and Fig. S1).

To investigate whether the identified sites would enable disulfide bond formation between FVIIa and sTF, a subset of five pairs sampling the entire interface were transiently coexpressed (Fig. 1*A*). Subsequent analysis of culture supernatants by consecutive rounds of TF immunoprecipitation (IP) and FVII staining identified a distinct 98-kDa band in four of the five coexpressions, corresponding to the predicted molecular weight of the fully glycosylated covalent complex (Fig. 1*B*). In the case of the FVIIa–sTF complexes F40C-V207C (7TF-40), Q64C-G109C (7TF-64), and F275C-W45C (7TF-275) expression levels were estimated to be on par with that of free FVII.

Immunostaining for FVII and sTF in the culture medium of a cell line stably expressing 7TF-64 showed the cross-linking to be driven to completion by sTF G109C expressed in excess over FVIIa Q64C (Fig. 1*C*). Since the Gla domain is in direct contact with sTF in the FVIIa+sTF complex (3), we asked whether covalent complex formation would be dependent on Gla domain maturation taking place during transit through the secretory pathway. To this end, 7TF-64 was expressed in the presence of vitamin K or warfarin to promote or antagonize γ-carboxylation, respectively. Probing of culture supernatants and cell lysates demonstrated comparable levels of complex in the samples under both conditions (Fig. 1*D*). In contrast, only cell culture supernatants from vitamin K-treated cells contained complex that could be detected by an antibody specific for the γ-carboxylated and calcium-complexed Gla-domain (30) (Fig. 1*D*). Thus, complex formation appeared to occur intracellularly and independent of γ-carboxylation.

**Probing the Conformational State of FVIIa in Covalent Complex with sTF.** The three most abundantly expressed complexes (i.e., 7TF-40, -64, and -275) (Fig. 1*B*) were purified as zymogens. In line with previous observations on the noncovalent complex (31), they did not autoactivate in solution, but were readily activated into three-chain species upon exposure to FIXa. Electrophorectic mobilities under reducing conditions corresponded to those of free FVIIa and sTF, indicating normal glycosylation of the complexes (Fig. 1*E*).

To determine the conformational activation state of the protease domain in the complexes, their intrinsic catalytic activities were measured. Using a chromogenic peptide substrate the estimated $k_{cat}/K_M$ values of 7TF-40 and -64 were found to be indistinguishable from that of FVIIa saturated with sTF, whereas the activity of 7TF-275 was twofold lower due to a compromised $K_M$ (Table 1 and Fig. S2). Probing of the S1 pocket with *p*-aminobenzamidine (pABA) similarly demonstrated a twofold increased inhibition constant ($K_i$) for 7TF-275, suggesting that its active site was not fully matured (Table 1 and Fig. S3). This appeared to be the result of an incomplete zymogen to enzyme transition as 7TF-275, unlike the other disulfide complexes and FVIIa+sTF, was recognized by the zymogen conformation-specific antibody F3-3.2a (10) and also reacted readily with potassium cyanate (KOCN), indicative of incomplete insertion of I153 into the activation pocket (Fig. 2 *A* and *B*).

To further assess the degree of productive interactions between FVIIa and sTF in the complexes, proteolytic activities toward the macromolecular substrate FX were determined in the

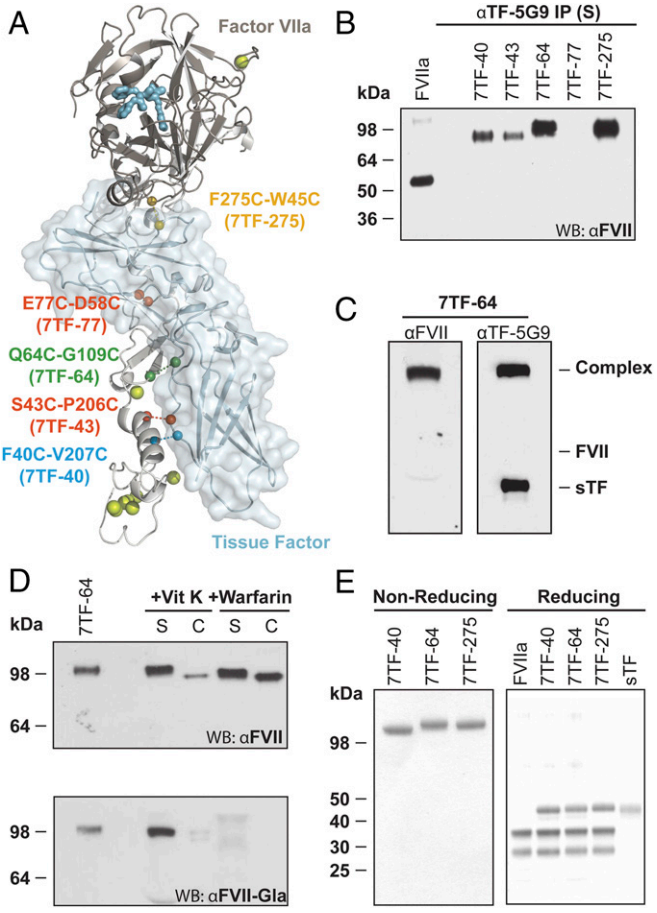


**Fig. 1.** Design and expression of disulfide-linked FVIIa–sTF complexes. (*A*) Crystal structure of the FVIIa+sTF complex (3) with the position of the five residue pairs targeted for cysteine replacement marked by spheres and interconnecting dashed lines. Labels refer to the mutation introduced in FVIIa and sTF, respectively. Calcium ions (yellow) and the active site inhibitor (light blue) are shown. (*B*) Each variant pair was transiently coexpressed in CHO cells and the culture supernatant analyzed 48 h posttransfection. Immediately after harvest, the culture supernatants were treated with 10 mM EDTA and 5 mM *N*-ethylmaleimide to dissociate any noncovalent complexes and block free thiols. Disulfide-linked complexes were detected by IP of the culture supernatant with anti-TF antibody (αTF-5G9) (51) followed by nonreducing SDS/PAGE and immunodetection of FVII with a polyclonal antibody (αFVII). (*C*) Immunostaining for FVII and sTF in the culture supernatant of a BHK cell line stably expressing 7TF-64 at 48 h after medium exchange. (*D*) Detection of complex formation in culture supernatants (S) and cell extracts (C) of 7TF-64–expressing BHK cells cultured for 24 h in the presence of vitamin $K_3$ or warfarin (25 μM) to promote or prevent γ-carboxylation, respectively. (*Upper*) Detection of FVII with αFVII after IP with αTF-5G9. (*Lower*) Detection with monoclonal antibody against the $Ca^{2+}$-complexed Gla-domain [αFVII-Gla (30)] after acetone precipitation. The amount loaded in lanes 3–5 were four times that of lane 2. (*E*) Reducing and nonreducing SDS/PAGE analysis of purified 7TF-40, 7TF-64, and 7TF-275 complexes followed by Coomassie staining. Where indicated, FVIIa or HEK293F-derived sTF were included for comparison.

**Table 1. Substrate and inhibitor reactivity of FVIIa–sTF complexes**

| Name | Mutations (FVIIa–sTF) | Amidolytic activity | | pABA inhibition | AT inhibition | Proteolytic activity | | | | |
|---|---|---|---|---|---|---|---|---|---|---|
| | | | | | | In solution | | On phospholipid vesicles | | |
| | | $k_{cat}/K_M$ ($mM^{-1}$ $s^{-1}$) | Relative activity* | $K_i$ (μM) | $k_{inh}$ ($M^{-1}s^{-1}$) | $k_{cat}/K_M$ ($M^{-1}$ $s^{-1}$) | Relative activity* | $K_M$ (nM) | $k_{cat}$ ($\times 10^{-4}$ $s^{-1}$) | Relative Activity* |
| FVIIa | None | 0.52 ± 0.01† | 1 | 1,329 ± 33 | 100 ± 33 | 2.39 ± 0.02† | 1 | 617 ± 110 | 2.34 ± 0.3 | 1 |
| FVIIa+sTF | None | 25.5 ± 1.5 | 49 | 94 ± 3 | 4,400 ± 140 | 663 ± 4† | 277 | 82 ± 7 | 27,000 ± 800 | 87,000 |
| 7TF-40 | F40C - V207C | 25.7 ± 1.3 | 49 | 92 ± 3 | N.D. | 119 ± 2† | 50 | 174 ± 37 | 290 ± 30 | 442 |
| 7TF-64 | Q64C - G109C | 26.6 ± 1.2 | 51 | 92 ± 3 | 4,400 ± 150 | 647 ± 2† | 271 | 71 ± 11 | 21,000 ± 1,100 | 78,000 |
| 7TF-275 | F275C - W45C | 13.5 ± 1.4 | 26 | 178 ± 9 | N.D. | 149 ± 4† | 63 | 87 ± 8 | 8,500 ± 200 | 25,700 |
| 7TF-64z | Q64C M306D - G109C | 0.89 ± 0.02† | 1.7 | N.D. | 160 ± 48 | 19.4 ± 0.2† | 9 | 201 ± 21 | 1,900 ± 100 | 2,400 |

Enzyme kinetic parameters and inhibition constants were measured as detailed in *Materials and Methods* (see also Figs. S2–S5) and are reported as mean ± SD ($n$ = 3) or relative to FVIIa. N.D., not determined.
*Catalytic activity ($k_{cat}/K_M$) relative to the activity of FVIIa in the absence of sTF.
†$k_{cat}/K_M$ values determined by linear regression at [S] << $K_M$.

absence or presence of phospholipid membrane. In solution, only 7TF-64 exhibited activity comparable to the noncovalent wild-type complex, whereas the $k_{cat}/K_M$ values for 7TF-40 and -275 were reduced by 5.6- and 4.5-fold, respectively (Table 1 and Fig. S4). An even more aggravated picture emerged in the presence of phospholipid vesicles, where the activities of FVIIa+sTF and 7TF-64 were 87,000- and 78,000-fold higher than FVIIa compared with 442- and 25,700-fold in the case of 7TF-40 and -275, respectively (Table 1). Further analysis revealed that the proteolytic activity of the 7TF-40 complex in solution could be restored to FVIIa+sTF levels when using a FX variant devoid of the Gla domain (Fig. 2*C*). This suggested that the impaired recognition of the full-length substrate occurred as a result of perturbations in the vicinity of the F40C-V207C linkage. This was, however, not the case for 7TF-275 in line with the location of this disulfide cross-link in the protease domain region (Fig. 2*C*). Taken together, these data showed that 7TF-64 closely recapitulated the conformation and functional properties of the FVIIa+sTF complex, whereas the two other complexes suffered from one or more defects likely localized to the site of disulfide linkage.

**Dismantling the Allosteric Stimulation of FVIIa in the 7TF-64 Complex.** The in vivo efficacy of FVIIa is dependent on its activity and lifetime in the blood stream. To address the latter aspect, the inhibition of 7TF-64 by AT was investigated as this pathway accounts for the major part of the clearance of active FVIIa (32). In the presence of low-molecular weight heparin, 7TF-64 was found to react 44-fold faster with AT compared with free FVIIa (Table 1 and Fig. S5). The similar increases in AT reactivity and amidolytic activity of 7TF-64 relative to FVIIa are consistent with AT inhibition being predominantly driven by active-site interactions in contrast to the surface-dependent recognition of macromolecular substrates (33). Based on this, we hypothesized that disruption of the allosteric transmission in 7TF-64 by introduction of the previously identified M306D mutation (15) would diminish the susceptibility to inhibition while maintaining proteolytic activity, and thus overall improve its pharmacodynamic properties.

Unlike the parent complex, 7TF-64 M306D (7TF-64z) exhibited amidolytic activity, F3-3.2a binding, and inactivation by KOCN similar to free FVIIa, which indicated a reversal of the protease domain conformation to a zymogen-like state (Fig. 2 *A* and *B* and Table 1). Consistent with this, the AT reactivity of 7TF-64z was only 1.6-fold higher than FVIIa (Table 1). Importantly, 7TF-64z retained a 2,400-fold higher proteolytic activity ($k_{cat}/K_M$) compared with FVIIa when FX activation was measured in the presence of a phospholipid surface, whereas the activation of FX in solution was only nine times greater than FVIIa measured under the same conditions (Table 1).

**Superior Pharmacodynamics of 7TF-64z.** The activity ranking of 7TF-64 and -64z was confirmed by standard activated partial thromboplastin time (aPTT) (Fig. S6) and by thromboelastography (TEG) in human whole blood using recalcification as a trigger. Under conditions mimicking hemophilia A, the apparent $EC_{50}$ value of 7TF-64z (4.4 ± 1.3 pM) was 90 times lower than that of FVIIa (0.40 ± 0.33 nM), while the parent complex 7TF-64 (0.10 ± 0.03 pM) was further reduced by 44-fold (Fig. 3*A*).

To assess the degree of membrane-dependency of the complexes under these conditions, the effect of a FVIIa Gla-domain specific antibody on calcium-triggered clot formation was investigated. In accordance with its recognition of the N-terminal ω-loop of the Gla domain (34, 35), this antibody did not affect FX activation in

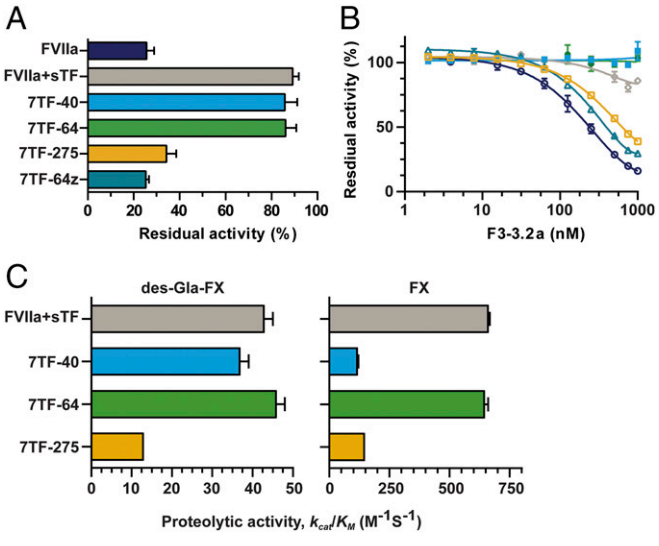


**Fig. 2.** Activation state of FVIIa in covalent complex with sTF. (*A*) Residual amidolytic activity of FVIIa and FVIIa–sTF complexes following exposure to 0.2 M KOCN for 2 h to assess the extent of I153 burial. (*B*) Residual amidolytic activity relative to antibody-free sample of FVIIa (○), FVIIa+sTF (◇), 7TF-40 (■), 7TF-64 (●), 7TF-275 (□), or 7TF-64z (Δ) following incubation with increasing concentrations of the zymogen conformation-specific inhibitory antibody F3-3.2a (10). (*C*) Catalytic constants ($k_{cat}/K_M$) for the activation of des-Gla FX (1.3 mM calcium) and FX (10 mM calcium) in solution. Results are shown as mean ± SD ($n$ = 3).

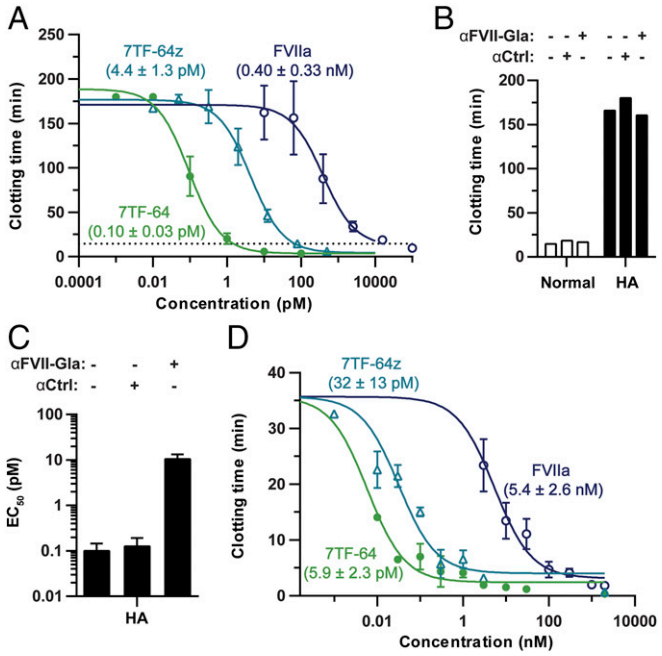


**Fig. 3.** Potencies of FVIIa–sTF complexes in human and murine hemophilia A whole blood. (*A*) Effect of of FVIIa (○), 7TF-64 (●), or 7TF-64z (Δ) on clotting times (mean ± SD, $n = 3$) in recalcified human whole blood depleted for FVIII by addition of a neutralizing antibody. From the concentration-response profiles, $EC_{50}$-values of 0.40 ± 0.33 nM, 0.10 ± 0.03 pM, and 4.4 ± 1.3 pM, respectively, were estimated. (*B*) Effect of 5 μM FVII Gla-domain–specific antibody (αFVII-Gla) (34) and an isotype control antibody (αCtrl) on clotting times in normal or FVIII-deficient whole blood from one representative donor. (*C*) The effect of 5 μM αFVII-Gla or αCtrl antibody on $EC_{50}$-values based on clotting time for 7TF-64 in FVIII deficient whole blood (mean ± SD, $n = 3$). (*D*) Effect of FVIIa (○), 7TF-64 (●), or 7TF-64z (Δ) on clotting times in recalcified murine hemophilia A whole blood (mean ± SD, $n = 4$). $EC_{50}$-values of 5.4 ± 2.6 nM, 5.9 ± 2.3 pM, and 32 ± 13 pM, respectively, were estimated from the concentration-response profiles.

solution but exhibited a dose-dependent inhibition of FX activation in the presence of phospholipid vesicles (Fig. S7). This property enabled a dissection of the procoagulant activity of the complexes into membrane-dependent and -independent contributions. Consistent with contact pathway-initiated clot formation, no effect of the antibody was observed under normal and hemophilia A conditions in the absence of added complex (Fig. 3*B*). On the other hand, in the presence of 7TF-64, representing the most procoagulant complex, supplementation of hemophilia A-like whole blood with 5 μM of the antibody increased the apparent $EC_{50}$ of 7TF-64 by two orders-of-magnitude (Fig. 3*C*). With a dissociation constant of 43 ± 2 nM for the antibody–7TF-64 interaction, this corresponded closely to the predicted change in $EC_{50}$, based on the level of unbound 7TF-64 that would exist under these conditions (Fig. S7). Consequently, a major part of the procoagulant effect of the complex could be attributed to its membrane-localized activity.

Dose titrations in hemophilia A ($F8^{-/-}$) mouse blood provided the same relative potency ranking of 7TF-64, -64z, and FVIIa, and thus qualified this model for evaluation of in vivo hemostatic effect (Fig. 3*D*). Following induction of vascular injury by tail-tip transection, vehicle-treated hemophilia A mice bled for the entire 30-min observation window. The bleeding phenotype could be corrected by administration of 300 nmol/kg FVIIa 5 min before injury, whereas 30 nmol/kg was inadequate (Fig. 4). Interestingly, administration of 7TF-64 at doses guided by its ex vivo potency only resulted in a correction of the blood loss at the highest tested dose of 4 nmol/kg. In contrast, a significantly improved hemostatic effect of 7TF-64z was observed with complete normalization of bleeding down to a dose of 0.3 nmol/kg, while 0.03 nmol/kg failed to normalize bleeding (Fig. 4). Platelet counts recorded at the end of the observation period were in all cases comparable to vehicle-treated control animals (Fig. S8). This was corroborated in a follow-up study, where neither platelet counts nor levels of thrombin–antithrombin complexes (TAT) were observed to significantly deviate from those of vehicle-treated control mice in a 24-h time window after administration of a normalizing dose (0.3 nmol/kg) of 7TF-64z (Fig. S9).

## Discussion

Introduction of disulfides is a commonly pursued approach to stabilize proteins. During the last decade, several computational tools have been developed that allow for prediction of positions amenable to cystine engineering based on a geometric analysis of input structures (reviewed in ref. 36). However, the use of static structures obtained by, for example, crystallography, does not take into account the dynamic conditions prevailing in solution. For this reason, prediction algorithms have been combined with ensemble-based approaches, such as MD, to simulate this aspect (37, 38). The usefulness of this approach was corroborated in the present study and extended to protein–protein interfaces. By taking backbone dynamics into account, a nonperturbing cystine bridge (Q64C-G109C) between FVIIa and sTF was found, which escaped identification using the crystal structure of the complex. In fact, seven of the nine predicted cross-links based on the MD approach were missed in the analysis of the crystal or energy-minimized structure of FVIIa+sTF due to unfavorable backbone geometries (Fig. S1).

Of the five cysteine pairs tested, four were found to mediate spontaneous assembly of FVIIa and sTF into disulfide-linked complexes. Among these, only 7TF-64 retained the functional properties of the noncovalent wild-type complex. The reason for the apparent difficulty in reliably predicting this feature is unclear. However, it is of interest to note that the nonperturbing disulfide in 7TF-64 is structurally incompatible with any of the more than 30 deposited crystal structures of FVIIa+sTF (39). This may suggest that the interface in the wild-type complex is undergoing a greater degree of structural fluctuation than appreciated from the ensemble of available crystal structures. If required for productive FX engagement, restrained motion in certain regions of the complexes as a result of cross-linking could contribute to the defects observed in

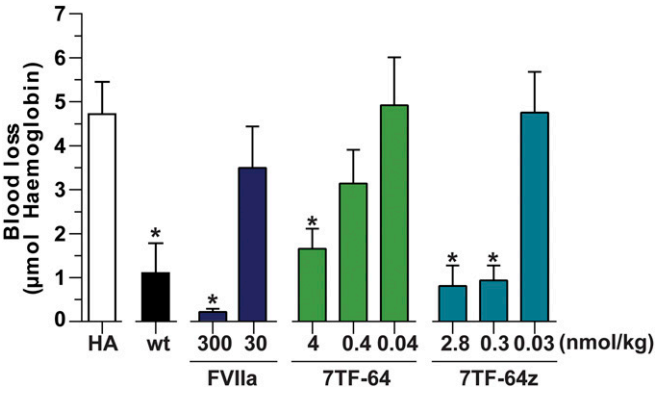


**Fig. 4.** Effect of FVIIa and FVIIa–sTF complexes on tail bleeding in hemophilia A mice. Fully anesthetized hemophilia A mice were administered the indicated amounts of FVIIa, 7TF-64, or 7TF-64z at 5 min before tail-tip transection. Blood loss was determined from the amount of hemoglobin (μmol) collected in the following 30 min. Vehicle-treated hemophilia A and normal mice (wild-type) were included for comparison. Results are shown as mean ± SEM ($n = 5$ or greater). Asterisks indicate samples for which the blood loss was significantly different ($P < 0.05$) from vehicle treated hemophilia A controls as determined by one-way ANOVA followed by a Bonferroni test for significance.

the assembled but poorly active complexes. Indeed, using a truncated FX as substrate, the defect in 7TF-40 could be localized to the region of disulfide introduction.

Analysis of cell lysates showed the assembly of 7TF-64 to occur intracellularly and independent of Gla-domain maturation. This finding is consistent with an only minor contribution of the Gla-domain to the high-affinity interaction of FVIIa with sTF (40). Together with an increased local concentration of the proteins in the secretory pathway and irreversibility of disulfide formation, this might explain the observed high efficiency of complex assembly by the coexpression procedure.

Inhibition by AT constitutes the major clearance pathway of active FVIIa in vivo accounting for ∼65% of its total clearance (32). Following administration of FVIIa to humans, the rate of inhibition by AT ($k_{inh}$ 34 $M^{-1}s^{-1}$) (32) has been estimated to be ∼30 times faster than that measured in vitro in the absence of cofactors (12, 14). Potentiation of AT by endogenous heparin-like glycosaminoglycans has been suggested to account for this difference (41). Conformational activation of FVIIa by TF also accelerates the inhibition by AT and is evident as a 44-fold faster inhibition of 7TF-64 compared with free FVIIa. Assuming additivity of the two effects as supported by in vitro studies (14), the half-life of 7TF-64 is estimated to be around 3 min in the human circulation when disregarding the contribution from other clearance pathways. This is significantly shorter than the half-life of FVIIa (2–3 h) (32) and would greatly limit the applicability of 7TF-64 as a hemostatic agent.

To alleviate the rapid inactivation of 7TF-sTF by AT, the M306D mutation was introduced to disconnect the allosteric signal from sTF to FVIIa (15). The retained efficiency of this mutation in the context of the covalent complex was evident from a rate of carbamylation and recognition by F3-3.2a similar to free FVIIa. Consequently, the conformation of FVIIa in 7TF-64z appeared to closely resemble that of the zymogen-like free form, but with all exosites in place for efficient substrate engagement. This was further substantiated by the observation that the 27- to 30-fold reduction in amidolytic activity and AT reactivity of 7TF-64z relative to 7TF-64 closely matched the relative loss of proteolytic activity with or without phospholipids (33- and 30-fold, respectively). In solution, the proteolytic activity of 7TF-64z was only nine times greater than FVIIa, consistent with most of the stimulation by sTF originating from allosteric effects under these conditions (15). In contrast, membrane-localization of the complex allowed for the realization of exosite interactions, resulting in a 2,400-fold increase in activity relative to FVIIa tested under identical conditions. If the remaining small increase in the amidolytic activity of 7TF-64z compared with FVIIa is adjusted for, we find that exosite interactions are responsible for an estimated 1,400-fold increase in the membrane-dependent proteolytic activity of FVIIa when bound to sTF. Compared with the 30- to 50-fold increase in activity, which can be obtained by mutations promoting the allosteric transition in FVIIa (6, 25), it is clear that exosite optimization holds a superior potential in the engineering of superactive FVIIa variants. As demonstrated in hemophilia A whole blood, this approach also serve to localize activity to the procoagulant membrane surface and thus confine action in a spatial manner to the site of injury (Fig. 3). In addition, 7TF-64z was found to retain susceptibility to FXa-dependent inhibition by tissue factor pathway inhibitor (TFPI), suggesting that the complex might be subjected to an additional layer of temporal regulation by this physiological inhibitor of the FVIIa–TF complex (42) (Fig. S10).

Considering that allosteric stimulation only constitutes a small fraction of the TF-driven activity enhancement of FVIIa toward FX, it raises the question of the physiological importance of this mechanism in the initiation of coagulation. With the availability of genome-editing tools allowing for the introduction of specific point mutations in the FVII gene (43), this aspect could be addressed experimentally in suitable animal models by taking advantage of the M306D mutation.

In FVIII-neutralized human and mouse whole blood, the enhanced proteolytic activity of 7TF-64z translated into an ∼100 times higher potency ($EC_{50}$) compared with FVIIa. Combined with an expected in vivo half-life of 1–2 h according to the measured AT reactivity, 7TF-64z appeared to have a profile suitable for acute treatment of bleeds in hemophilia. To test this hypothesis, the tail-transection model in hemophilia A mice was employed (44). In this model, 300 nmol/kg (i.e., 15 mg/kg) FVIIa restored the bleeding phenotype when administered 5 min before injury. In the case of 7TF-64, an unexpectedly high dose of 4 nmol/kg was needed to correct bleeding. With a conservatively estimated half-life in plasma of around 3 min, this likely reflects the need for additional 7TF-64 to compensate for its fast elimination. The 7TF-64z complex, on the other hand, was found to be highly effective with normalization achieved at doses down to 0.3 nmol/kg. Notably, unperturbed platelet counts and TAT levels were observed for 7TF-64z up to 24-h postadministration, suggesting the absence of systemic coagulation and thus consistent with the platelet-localized activity of the complexes demonstrated in vitro.

In a therapeutic context, immunogenicity constitutes another risk factor. According to in silico T-cell epitope prediction (45, 46), the introduced cysteine mutations appear benign, whereas M306D maps to a segment of predicted risk (Fig. S11). Furthermore, while 7TF-64z possesses impressive efficacy in an acute setting, additional improvement of its duration of action or therapeutic index will be required to be applicable in a prophylaxis setting relying on regular but infrequent administrations.

In conclusion, we have shown that disulfide-mediated cofactor cross-linking represents a viable route to a potent exosite-controlled procoagulant FVIIa molecule. Since the modulation of proteolytic function by protein–protein interactions is widespread in nature, the strategy outlined in the present study may have general applicability in the tailoring of proteolytic function for specific purposes.

## Materials and Methods

**Cofactors and Buffers.** Recombinant sTF (1–219) was derived from *Escherichia coli* (15, 20) unless otherwise stated. FVIIa was from Novo Nordisk A/S. L-α-phosphatidylcholine (chicken egg) and L-α-phosphatidylserine (porcine brain) from Avanti Polar Lipids were used for the preparation of 10:90 PS:PC vesicles according to published procedures (47).

Unless otherwise stated, experiments were performed in HBS buffer (20 mM Hepes, 100 mM NaCl, pH 7.4) at room temperature and data were analyzed using GraphPad Prism.

**Animals.** Mice genetically deficient in FVIII ($F8^{-/-}$ C57BL/6J) were originally obtained from Bi et al. (48) and bred at Taconic. Normal C57BL/6J mice were obtained from Taconic. The animals were between 12 and 16 wk, with an equal distribution of males and females. All experiments were approved by and performed according to guidelines from The Danish Animal Experiments Council, the Danish Ministry of Justice.

**Design of FVIIa–sTF Disulfide Complexes.** The crystal structure of FVIIa+sTF [PDB ID code 1DAN (3)] with the active-site inhibitor removed and 166 snapshots along a 20-ns MD trajectory of the same complex (49) were analyzed to identify positions for disulfide engineering according to Dombkowski (29). Predicted disulfides were modeled into the crystal structure of FVIIa+sTF using CHARMm (Accelrys Inc.) and the resulting geometries were analyzed. Finally, the models were energy minimized by 250 steps of conjugated gradient minimization in CHARMm (Fig. S1).

**Expression and Purification of FVIIa–sTF Complexes.** Transient coexpressions of FVIIa and sTF cysteine variants were performed in Chinese Hamster Ovary (CHO)-K1 cells using standard techniques. Purification and quantification of complexes expressed by stable Baby Hamster Kidney (BHK) cell lines (50) was performed by immuno-affinity chromatography (34) and active-site titration (33), as previously described. See *SI Materials and Methods* for detailed experimental protocols.

**Functional Evaluation of Disulfide Complexes.** Peptide substrate hydrolysis (S-2288; Chromogenix), competitive inhibition by pABA, chemical modification of the N-terminal I153 (15, 20), and inhibition by the zymogen conformation-specific antibody F3-3.2a (10) was conducted essentially as described elsewhere. Activation of FX and des-gla FX in solution and on phospholipid vesicles (10:90 PS:PC) were carried out as detailed in refs. 15 and 20. Kinetics of inhibition by human plasma-derived AT was determined under pseudofirst-order conditions in the presence of low molecular weight heparin, as described elsewhere (33). See *SI Materials and Methods* for detailed experimental protocols.

**Ex Vivo Potencies in Human and Murine Hemophilia A Whole Blood.** Clot formation was measured by thromboelastography after recalcification of citrated whole blood supplemented with FVIIa, 7TF-64 or 7TF-64z. See *SI Materials and Methods* for detailed experimental protocols.

**Hemostatic Effect in the Tail-Clip Model in Hemophilia A Mice.** The hemostatic effect of FVIIa, 7TF-64, and 7TF-64z was investigated using the tail bleeding model in hemophilia A mice, as previously described (44). See *SI Materials and Methods* for a detailed experimental protocol.

**ACKNOWLEDGMENTS.** The authors thank Anette W. Bruun, Lene L. Clausen, Carsten la Cour Christoffersen, and Birgitte Klitgaard for expert technical assistance. A.L.N. and A.B.S. were supported by the Danish Ministry of Science and Technology under the Industrial PhD program and the Novo Nordisk R&D Science Talent Attraction and Recruitment program. W.R. is supported by NIH Grant HL-60742.

1. Mann KG, Butenas S, Brummel K (2003) The dynamics of thrombin formation. *Arterioscler Thromb Vasc Biol* 23:17–25.
2. Gajsiewicz JM, Morrissey JH (2015) Structure-function relationship of the interaction between tissue factor and factor VIIa. *Semin Thromb Hemost* 41:682–690.
3. Banner DW, et al. (1996) The crystal structure of the complex of blood coagulation factor VIIa with soluble tissue factor. *Nature* 380:41–46.
4. McCallum CD, Hapak RC, Neuenschwander PF, Morrissey JH, Johnson AE (1996) The location of the active site of blood coagulation factor VIIa above the membrane surface and its reorientation upon association with tissue factor. A fluorescence energy transfer study. *J Biol Chem* 271:28168–28175.
5. Baugh RJ, Dickinson CD, Ruf W, Krishnaswamy S (2000) Exosite interactions determine the affinity of factor X for the extrinsic Xase complex. *J Biol Chem* 275:28826–28833.
6. Ruf W, Kalnik MW, Lund-Hansen T, Edgington TS (1991) Characterization of factor VII association with tissue factor in solution. High and low affinity calcium binding sites in factor VII contribute to functionally distinct interactions. *J Biol Chem* 266:15719–15725.
7. Fiore MM, Neuenschwander PF, Morrissey JH (1994) The biochemical basis for the apparent defect of soluble mutant tissue factor in enhancing the proteolytic activities of factor VIIa. *J Biol Chem* 269:143–149.
8. Bom VJ, Bertina RM (1990) The contributions of Ca2+, phospholipids and tissue-factor apoprotein to the activation of human blood-coagulation factor X by activated factor VII. *Biochem J* 265:327–336.
9. Higashi S, Matsumoto N, Iwanaga S (1996) Molecular mechanism of tissue factor-mediated acceleration of factor VIIa activity. *J Biol Chem* 271:26569–26574.
10. Dickinson CD, Shobe J, Ruf W (1998) Influence of cofactor binding and active site occupancy on the conformation of the macromolecular substrate exosite of factor VIIa. *J Mol Biol* 277:959–971.
11. Huber R, Bode W (1978) Structural basis of the activation and action of trypsin. *Acc Chem Res* 11:114–122.
12. Lawson JH, Butenas S, Ribarik N, Mann KG (1993) Complex-dependent inhibition of factor VIIa by antithrombin III and heparin. *J Biol Chem* 268:767–770.
13. Higashi S, Nishimura H, Aita K, Iwanaga S (1994) Identification of regions of bovine factor VII essential for binding to tissue factor. *J Biol Chem* 269:18891–18898.
14. Olson ST, et al. (2004) Accelerating ability of synthetic oligosaccharides on antithrombin inhibition of proteinases of the clotting and fibrinolytic systems. Comparison with heparin and low-molecular-weight heparin. *Thromb Haemost* 92:929–939.
15. Persson E, Nielsen LS, Olsen OH (2001) Substitution of aspartic acid for methionine-306 in factor VIIa abolishes the allosteric linkage between the active site and the binding interface with tissue factor. *Biochemistry* 40:3251–3256.
16. Dickinson CD, Ruf W (1997) Active site modification of factor VIIa affects interactions of the protease domain with tissue factor. *J Biol Chem* 272:19875–19879.
17. Ruf W, et al. (1999) Importance of factor VIIa Gla-domain residue Arg-36 for recognition of the macromolecular substrate factor X Gla-domain. *Biochemistry* 38:1957–1966.
18. Dickinson CD, Kelly CR, Ruf W (1996) Identification of surface residues mediating tissue factor binding and catalytic function of the serine protease factor VIIa. *Proc Natl Acad Sci USA* 93:14379–14384.
19. Ruf W, Miles DJ, Rehemtulla A, Edgington TS (1992) Cofactor residues lysine 165 and 166 are critical for protein substrate recognition by the tissue factor-factor VIIa protease complex. *J Biol Chem* 267:6375–6381.
20. Andersen LM, et al. (2012) Antibody-induced enhancement of factor VIIa activity through distinct allosteric pathways. *J Biol Chem* 287:8994–9001.
21. Gouw SC, van der Bom JG, Marijke van den Berg H (2007) Treatment-related risk factors of inhibitor development in previously untreated patients with hemophilia A: The CANAL cohort study. *Blood* 109:4648–4654.
22. Hoffman M, Monroe DM, 3rd (2001) The action of high-dose factor VIIa (FVIIa) in a cell-based model of hemostasis. *Semin Hematol* 38(4, Suppl 12):6–9.
23. Augustsson C, Persson E (2014) In vitro evidence of a tissue factor-independent mode of action of recombinant factor VIIa in hemophilia. *Blood* 124:3172–3174.
24. Keshava S, Sundaram J, Rajulapati A, Pendurthi UR, Rao LVM (2016) Pharmacological concentrations of recombinant factor VIIa restore hemostasis independent of tissue factor in antibody-induced hemophilia mice. *J Thromb Haemost* 14:546–550.
25. Persson E, Kjalke M, Olsen OH (2001) Rational design of coagulation factor VIIa variants with substantially increased intrinsic activity. *Proc Natl Acad Sci USA* 98:13583–13588.
26. Mahlangu JN, et al. (2012) Phase I, randomized, double-blind, placebo-controlled, single-dose escalation study of the recombinant factor VIIa variant BAY 86-6150 in hemophilia. *J Thromb Haemost* 10:773–780.
27. Lentz SR, et al.; adept™2 investigators (2014) Recombinant factor VIIa analog in the management of hemophilia with inhibitors: Results from a multicenter, randomized, controlled trial of vatreptacog alfa. *J Thromb Haemost* 12:1244–1253.
28. Harvey SB, Stone MD, Martinez MB, Nelsestuen GL (2003) Mutagenesis of the gamma-carboxyglutamic acid domain of human factor VII to generate maximum enhancement of the membrane contact site. *J Biol Chem* 278:8363–8369.
29. Dombkowski AA (2003) Disulfide by Design: A computational method for the rational design of disulfide bonds in proteins. *Bioinformatics* 19:1852–1853.
30. Kazama Y, Pastuszyn A, Wildgoose P, Hamamoto T, Kisiel W (1993) Isolation and characterization of proteolytic fragments of human factor VIIa which inhibit the tissue factor-enhanced amidolytic activity of factor VIIa. *J Biol Chem* 268:16231–16240.
31. Neuenschwander PF, Morrissey JH (1992) Deletion of the membrane anchoring region of tissue factor abolishes autoactivation of factor VII but not cofactor function. Analysis of a mutant with a selective deficiency in activity. *J Biol Chem* 267:14477–14482.
32. Agersø H, et al. (2011) Recombinant human factor VIIa (rFVIIa) cleared principally by antithrombin following intravenous administration in hemophilia patients. *J Thromb Haemost* 9:333–338.
33. Larsen KS, et al. (2007) Engineering the substrate and inhibitor specificities of human coagulation Factor VIIa. *Biochem J* 405:429–438.
34. Thim L, et al. (1988) Amino acid sequence and posttranslational modifications of human factor VIIa from plasma and transfected baby hamster kidney cells. *Biochemistry* 27:7785–7793.
35. Cheung WF, Wolberg AS, Stafford DW, Smith KJ (1995) Localization of a metal-dependent epitope to the amino terminal residues 33-40 of human factor IX. *Thromb Res* 80:419–427.
36. Dombkowski AA, Sultana KZ, Craig DB (2014) Protein disulfide engineering. *FEBS Lett* 588:206–212.
37. Pellequer J-L, Chen SW (2006) Multi-template approach to modeling engineered disulfide bonds. *Proteins* 65:192–202.
38. Wijma HJ, et al. (2014) Computationally designed libraries for rapid enzyme stabilization. *Protein Eng Des Sel* 27:49–58.
39. Berman HM, et al. (2000) The Protein Data Bank. *Nucleic Acids Res* 28:235–242.
40. Neuenschwander PF, Morrissey JH (1994) Roles of the membrane-interactive regions of factor VIIa and tissue factor. The factor VIIa Gla domain is dispensable for binding to tissue factor but important for activation of factor X. *J Biol Chem* 269:8007–8013.
41. Østergaard H, et al. (2014) Modulating the antithrombin-mediated in vivo clearance of coagulation factor VIIa. *Blood* 124:4233.
42. Girard TJ, et al. (1989) Functional significance of the Kunitz-type inhibitory domains of lipoprotein-associated coagulation inhibitor. *Nature* 338:518–520.
43. Sander JD, Joung JK (2014) CRISPR-Cas systems for editing, regulating and targeting genomes. *Nat Biotechnol* 32:347–355.
44. Holmberg HL, Lauritzen B, Tranholm M, Ezban M (2009) Faster onset of effect and greater efficacy of NN1731 compared with rFVIIa, aPCC and FVIII in tail bleeding in hemophilic mice. *J Thromb Haemost* 7:1517–1522.
45. Nielsen M, Justesen S, Lund O, Lundegaard C, Buus S (2010) NetMHCIIpan-2.0—Improved pan-specific HLA-DR predictions using a novel concurrent alignment and weight optimization training procedure. *Immunome Res* 6:9.
46. Nielsen M, Lund O (2009) NN-align. An artificial neural network-based alignment algorithm for MHC class II peptide binding prediction. *BMC Bioinformatics* 10:296.
47. Smith SA, Morrissey JH (2004) Rapid and efficient incorporation of tissue factor into liposomes. *J Thromb Haemost* 2:1155–1162.
48. Bi L, et al. (1995) Targeted disruption of the mouse factor VIII gene produces a model of haemophilia A. *Nat Genet* 10:119–121.
49. Olsen OH, Rand KD, Østergaard H, Persson E (2007) A combined structural dynamics approach identifies a putative switch in factor VIIa employed by tissue factor to initiate blood coagulation. *Protein Sci* 16:671–682.
50. Persson E, Nielsen LS (1996) Site-directed mutagenesis but not gamma-carboxylation of Glu-35 in factor VIIa affects the association with tissue factor. *FEBS Lett* 385:241–243.
51. Ruf W, Rehemtulla A, Edgington TS (1991) Antibody mapping of tissue factor implicates two different exon-encoded regions in function. *Biochem J* 278:729–733.
52. Wildgoose P, et al. (1992) Measurement of basal levels of factor VIIa in hemophilia A and B patients. *Blood* 80:25–28.